One-dimensional Holstein model revisited

Sijia Zhao

Department of Applied Physics, Stanford University, Stanford, California 94305, USA

Zhaoyu Han and Steven A. Kivelson

Department of Physics, Stanford University, Stanford, California 94305, USA

Ilya Esterlis

Department of Physics, Harvard University, Cambridge, Massachusetts 02138, USA

We analyze the global ground-state (quantum) phase diagram of the one-dimensional spinful Holstein model at half filling as a function of the strength of the electron-phonon coupling (represented by the strength of the phonon-induced attraction, U) and the phonon frequency ω_0. In addition to reanalyzing the various asymptotic regimes, we carry out density-matrix renormalization group simulations to correct previous inferences concerning the antiadiabatic (large ω_0) and strong-coupling (large U) regimes. There are two distinct phases—a fully gapped commensurate charge-density-wave phase and a spin-gapped Luther-Emery phase with a gapless charge mode—separated by a phase boundary, with a shape that reflects different microscopic physics in the weak- and strong-coupling limits.

I. INTRODUCTION

The interaction between charge carriers and lattice vibration plays a fundamental role in strongly correlated quasi-one-dimensional (quasi-1D) materials [1–8]. The Holstein model [5,6] is probably one of the simplest microscopic models of coupled electrons and phonons, which makes it an ideal platform for exact numerical methods such as the density-matrix renormalization group (DMRG) [9–12], quantum Monte Carlo (QMC) [13–18], and other algorithms [19–21]. Surprisingly, there remain some long-standing debates, even for the 1D Holstein model at half filling, concerning basic facts about the structure of the zero-temperature ($T = 0$) phase diagram, as well as discrepancies in the critical values of couplings that mark the phase boundaries obtained with different numerical methods [13]. While early studies inferred a single ordered phase for any nonzero electron-phonon coupling and finite phonon retardation [17,22,23], more recent numerical results [9,10,12,13,15,16,24] have suggested the existence of a disordered phase and at least one phase boundary. Specifically, Hirsch and Fradkin [17] examined the behavior of the model as a function of ω_0, the bare phonon frequency, and U, the bipolaron binding energy, which is an appropriate characterization of the electron-phonon coupling strength, both measured in units of the electron bandwidth, $4|t|$. Based on topological constraints on the nature of the phase diagram and other considerations, they speculated that the phase diagram exhibits only one phase—a fully gapped, long-range-ordered charge-density-wave (CDW) phase—everywhere off these boundaries. They partially corroborated this conjecture with QMC studies, which were among the first such studies for a fermionic system.

In this paper, we revisit this problem and conclude that the correct quantum phase diagram for the half-filled 1D Holstein model is the one shown schematically in Fig. 1. In addition to the CDW phase, there is also a Luther-Emery (LE) phase, which has a spin gap but a gapless charge mode and CDW quasi-long-range order; that is, it resembles an incommensurate fluctuating CDW. This structure of the phase diagram is consistent with the topological arguments of Fradkin and Hirsch in that the phase boundary does not terminate on any of the edges of the phase diagram, but rather extends from the "corner" at $U = \omega_0 = 0$ to that at $U = \omega_0 \rightarrow \infty$. Effects of electron-electron repulsions have been ignored for the purposes of the present study.

In support of these conclusions, we have explored the behavior in the vicinity of the four edges of the phase diagram, each of the regions indicated by a different color of shading in Fig. 1. The analysis in the neighborhood of the upper ($\omega_0 = \infty$) and leftmost ($U = 0$) edges is subtle, as they correspond to quantum critical lines, and of course, the two corners of the phase diagram at which the phase boundary starts and ends are of particular interest.

(i) We have derived an effective Hamiltonian in powers of t/ω_0 and U/ω_0 that is valid in the vicinity of the $\omega_0 \rightarrow \infty$ (upper) edge of the phase diagram and then solved it using high-precision DMRG studies on very long (up to length $L = 400$) systems. We establish that the asymptotic equivalence between the CDW and LE correlations [i.e., the emergent SU(2) symmetry as $\omega_0 \rightarrow \infty$] is lifted for large but finite ω_0 so that there is a LE phase immediately below this edge of the phase diagram. This is in contrast to what was conjectured by Hirsch and Fradkin and is our most important result.
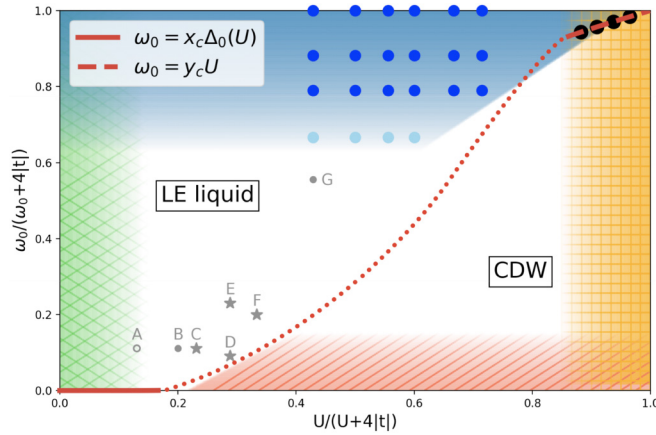
FIG. 1. Ground-state phase diagram of the 1D Holstein model. Both phases have a spin gap, $\Delta_s > 0$. The LE liquid phase has a gapless charge mode, while the CDW is fully gapped. Distinct asymptotic approaches apply at each edge of the phase diagrams: (i) In the blue (antiadiabatic) region, where $\omega_0 \gg |t|, U$, we have derived an effective Hamiltonian in powers of t/ω_0 and U/ω_0 and solved it using DMRG as denoted by the blue points. (ii) In the orange (strong-coupling) region, $U \gg |t|$, we use a combination of a strong-coupling expansion [25] and DMRG to numerically identify the position of the phase boundary, $\omega_0 \sim y_c U$, with $y_c \approx 0.45$, as indicated by the black circles. (iii) In the red (adiabatic) region, where $\omega_0 \ll \Delta_0$ and $|t|$, with $\Delta_0 = 4|t| \exp[-2\pi |t|/U]$ being the mean-field gap (for charge and spin), the CDW is stable against quantum fluctuations up to a critical value of ω_0. For small $U \ll t$, we estimate the critical phonon frequency to be $\omega_c \sim x_c \Delta_0$, with $x_c \approx 1$. (iv) In the green (weak-coupling) region, $U \ll |t|$, a previous functional renormalization group analysis [24] confirms an extended LE liquid phase. The solid portions of the phase boundary are drawn according to the asymptotic expressions obtained in the text; the dotted portion is a conjectural smooth interpolation between these end regions. The points labeled A–G refer to previous numerical studies (not our own), as discussed in the text, in which those indicated by an open circle, stars, and solid circles were argued to lie in a LE liquid, in a CDW, and on the phase boundary, respectively.

(ii) We consider a strong-coupling expansion of the model (originally derived by Freericks [25]) to fourth order in t/U to explore the right edge of the phase diagram. Again, we use high-precision DMRG studies to determine the behavior of this effective model, which (as was previously known) always has an ordered CDW phase if the limit $U \to \infty$ is taken at fixed ω_0. However, we find that for large but finite U, there is a phase transition from a CDW ordered state for $\omega_0 < y_c U$ to a LE liquid phase for $\omega_0 > y_c U$, where we estimate $y_c \approx 0.45$.

(iii) The familiar Peierls instability ensures that for any fixed $U > 0$, the ground state is an ordered CDW in the limit $\omega_0 \to 0$, i.e., on the lower boundary of the phase diagram. Specifically, for $\omega_0 = 0$, a mean-field analysis is exact, which predicts a finite gap $\Delta_0 = 4|t| \exp(-2\pi |t|/U)$ for both charge and spin modes.

(iv) The Fermi liquid state at $U = 0$ is perturbatively unstable (and in that sense is quantum critical) since weak attractive interactions inevitably lead to a state with a spin gap. For small U and ω_0, we present a field-theoretic analysis that suggests that the CDW state melts with increasing ω_0 at an exponen-

tially small value, $\omega_0 = x_c \Delta_0 \sim \exp(-2\pi |t|/U)$. Concerning larger values of ω_0, but still in this weak-coupling regime, we also briefly recap a previous functional renormalization group (RG) analysis [24] that shows the existence of a LE liquid phase everywhere proximate to the $U \to 0$ (left) edge of the phase diagram.

Along the way, we comment on the relation between our results and several other numerical studies [12,13,15] that have been carried out since the pioneering work of Fradkin and Hirsch. We also present arguments suggesting that the lightly doped system exhibits a single LE liquid phase for all ω_0 and $U \neq 0$.

II. THE MODEL

The Holstein model is defined as

$$\hat{H} = -t \sum_{\langle ij \rangle, \sigma} (\hat{c}_{i,\sigma}^\dagger \hat{c}_{j,\sigma} + \text{H.c.}) + \alpha \sum_i \hat{n}_i \hat{x}_i$$
$$+ \sum_i \left[\frac{\hat{p}_i^2}{2m} + \frac{K \hat{x}_i^2}{2} \right]. \tag{1}$$

The first term describes the hopping of electrons between nearest-neighbor sites $\langle ij \rangle$, where $\hat{c}_{i,\sigma}^\dagger$ creates an electron with spin polarization σ at site i. The second term describes the electron-phonon interaction, where $\hat{n}_i \equiv \sum_\sigma \hat{c}_{i,\sigma}^\dagger \hat{c}_{i,\sigma}$ is the electron density operator and α is the electron-phonon coupling parameter. The last term contains the lattice degrees of freedom, with $\hat{x}_i$ being an optical phonon coordinate at site i and $\hat{p}_i$ being the conjugate momentum. There are three independent energy scales in this problem: the electron bandwidth $4|t|$, phonon frequency $\omega_0 \equiv \sqrt{K/m}$, and an effective electron-phonon interaction strength $U \equiv \alpha^2/K$.

III. THE ANTIADIABATIC LIMIT, $\omega_0 \to \infty$

To derive an effective Hamiltonian that is valid in the $\omega_0 \gg |t|, U$ limit, we perform a unitary transformation $\hat{Q} = \Pi_i \exp[i\alpha \hat{p}_i \hat{n}_i/K]$, such that the transformed Hamiltonian $\hat{H}' = \hat{Q}^\dagger \hat{H} \hat{Q}$ reads [26]

$$\hat{H}' = -t \sum_{\langle ij \rangle, \sigma} (e^{i\alpha(\hat{p}_i - \hat{p}_j)/K} \hat{c}_{i,\sigma}^\dagger \hat{c}_{j,\sigma} + \text{H.c.})$$
$$- \frac{U}{2} \sum_i \hat{n}_i^2 + \sum_i \left[\frac{\hat{p}_i^2}{2m} + \frac{K \hat{x}_i^2}{2} \right]. \tag{2}$$

Then through direct perturbation theory up to second order, we derived the effective Hamiltonian in powers of $1/\omega_0$ for large phonon frequency:

$$\hat{H}_{\text{eff}} = -t \sum_{\langle ij \rangle, \sigma} (\hat{c}_{i,\sigma}^\dagger \hat{c}_{j,\sigma} + \text{H.c.}) - \frac{U}{2} \sum_i \hat{n}_i^2$$
$$- \frac{U}{\omega_0^2} \sum_n (\hat{j}_n - \hat{j}_{n-1})^2, \tag{3}$$

where $\hat{j}_n$ is the local current operator defined as

$$\hat{j}_n = it \sum_\sigma (\hat{c}_{n,\sigma}^\dagger \hat{c}_{n+1,\sigma} - \hat{c}_{n+1,\sigma}^\dagger \hat{c}_{n,\sigma}). \tag{4}$$
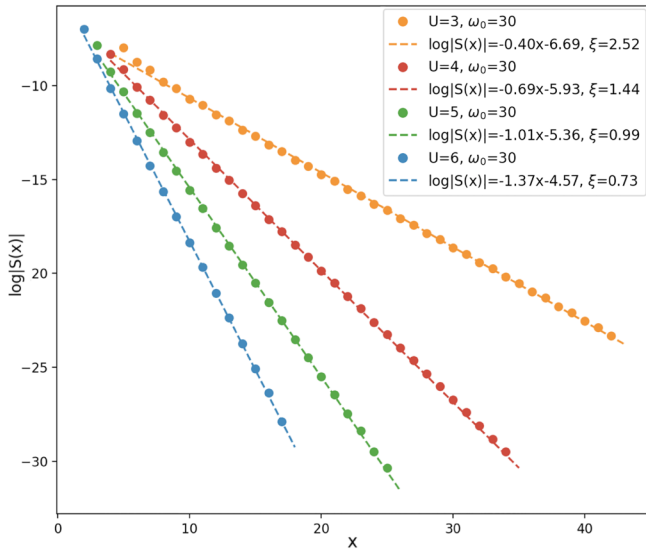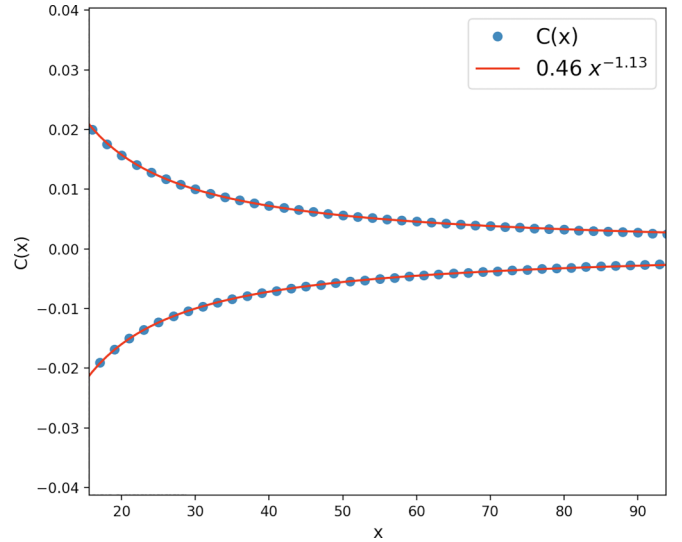
FIG. 2. Spin-spin correlations [Eq. (5)] with exponential fit.

FIG. 3. Charge-charge correlation [Eq. (7)] for $U = 6$ and $\omega_0 = 30$ at half filling. The Luttinger exponent is extracted using Eq. (8).

When $\omega_0 = \infty$, the effective model reduces to the attractive Hubbard model, while for large but finite ω_0, the leading-order correction gives a finite-range effective electron-electron interaction. Higher-order corrections to H_{eff} are of the order of $(t/\omega_0)^4$ and higher. The same effective Hamiltonian can be alternatively derived by a path integral representation. Detailed calculations are deferred to the Appendix A.

We determined ground-state properties of this effective Hamiltonian using DMRG studies on systems up to 400 sites long for values of ω_0 between 8 and ∞ and for values of U between 3 and 10. The values explored are indicated by the blue solid circles in the phase diagram in Fig. 1. All extracted quantities such as the Luttinger exponent K_c are obtained from the correlation function data that were extrapolated to infinite system size (see Fig. 14 for the details). The larger ω_0 results are more reliable since this is where the effective model best approximates the original problem. All the DMRG data collected are obtained from the lowest energy state out of five trials with independently randomized initial states, and all the results shown (unless otherwise stated) are extrapolated to zero truncation error, utilizing data collected with five truncation errors ranging from 1×10^{-7} to 9×10^{-7}. We have checked our results do not change significantly down to a truncation error of 1×10^{-10}, corresponding to keeping bond dimensions up to $m = 1500$. All data involving sites within $L/4$ to the open boundary are discarded; that is, we retain the data only in the interval $x \in [L/4, 3L/4]$ to reduce boundary effects.

Our findings can be summarized as follows; in all cases, we conclude that the system is in a LE phase, characterized by a spin gap and a single gapless charge mode. The presence of a spin gap is inferred from the fact that the spin-spin correlation function falls exponentially with distance, as shown in Fig. 2. Meanwhile, as shown in Fig. 3, the existence of a gapless charge mode follows from the observation that the charge-density correlations oscillate with wave vector π and have an amplitude that falls as a power of distance, i.e., as $e^{i\pi r}|r|^{-K_c}$. The inferred values of the charge Luttinger exponent K_c are

shown in Fig. 4 for all the values of U and ω_0 we have explored. As expected, $K_c \to 1$ as $\omega_0 \to \infty$, independent of U. Significantly, however, for a large but not infinite ω_0, we find that $K_c > 1$. This is an important consistency check, as umklapp scattering that could stabilize a long-range-ordered CDW phase is perturbatively irrelevant for $K_c > 1$ but would be relevant for $K_c < 1$.

We have carried out two further consistency checks of our results. We have computed the central charge, as shown in Fig. 5, and in all cases, we find values consistent with $c = 1$ within our uncertainty. This is the expected value for a LE liquid; these results are surely inconsistent with the $c = 0$ expected for a commensurate CDW with long-range order. We have also examined the nature of the state slightly away from the half-filled case. If commensurability effects are irrelevant
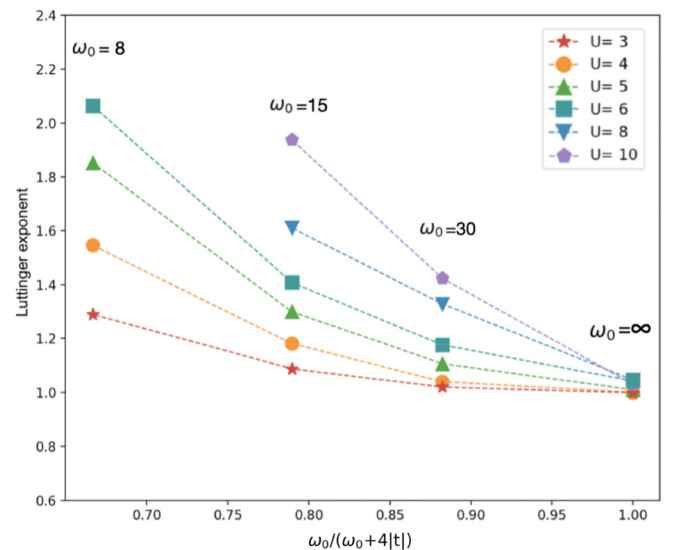
FIG. 4. A summary of Luttinger exponents for all values of (U, ω_0) that have been calculated by DMRG.
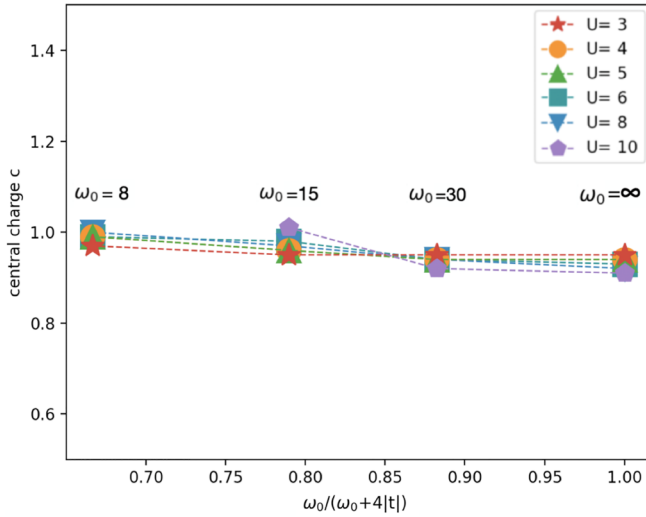
FIG. 5. The extracted central charge agrees well with $c = 1$ for all parameter points.

for $n = 1$, then the system is expected to evolve continuously with doping, $\delta \equiv 1 - n > 0$. Indeed, as shown in Figs. 6 and 7, we find that both the spin gap (or, more precisely, the correlation length characterizing the exponential falloff of the spin correlations) and the charge Luttinger exponent evolve continuously with δ. Were the system commensurate, we would expect a factor of 2 discontinuity in the spin gap and a jump of the Luttinger exponent to $K_c \approx 2$ for $0 < \delta \ll 1$.

A. Spin-spin correlation

We have computed the spin-spin correlation function, which is defined as

$$S(x) = \frac{1}{N_r} \sum_r [\langle S_z(r)S_z(r+x)\rangle - \langle S_z(r)\rangle\langle S_z(r+x)\rangle], \quad (5)$$

where $S_z(r)$ is the z component of the spin operator at site r and we have introduced an average over $N_r = 5$ "reference sites" near the center of the chain to reduce the finite-size effects. As shown in Fig. 2, it is clear that the spin correlators decay exponentially at large distances with a finite correlation length ξ extracted by fitting the large x decay of $S(x)$ to the asymptotic form

$$S(x) \sim A_S \exp[-x/\xi]. \quad (6)$$

The data presented in Fig. 2 are for $U = 3$, 4, 5, and 6, with $\omega_0 = 30$ and $L = 100$.

That similar long-range behavior has been found for all the values of ω_0 and U indicated in Fig. 1 confirms the noncontroversial expectation that there is a spin gap in the antiadiabatic limit for all U. A summary of ξ as a function of ω_0 for different values of U is shown in Fig. 8.

B. Density-density correlation

The charge correlation function is defined as

$$C(x) = \frac{1}{N_r} \sum_r [\langle n(r)n(r+x)\rangle - \langle n(r)\rangle\langle n(r+x)\rangle], \quad (7)$$
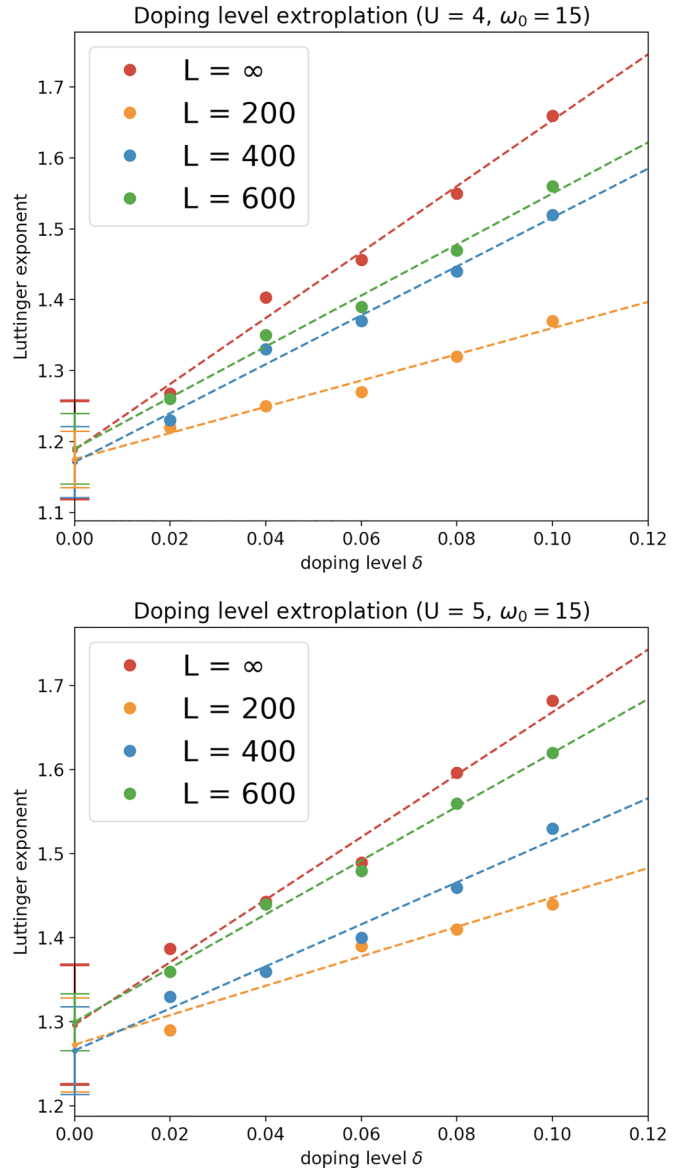

FIG. 6. K_C as a function of doping level δ, with error bars showing 95% confidence bounds for the intercepts. The extrapolated K_C at $\delta = 0$, i.e., the intercept of the fitting function, is 1.19 for $(U = 4, \omega_0 = 15)$ and 1.30 for $(U = 5, \omega_0 = 15)$. Both agree well with the values observed at half filling $(\delta = 0)$, as shown in Fig. 4.

where $n(r) \equiv \sum_\sigma n_\sigma(r)$ is the total density of electrons on site r and, again, we average over $N_r = 5$ reference sites. At large distances, we always find that $C(x)$ exhibits power-law behavior,

$$C(x) = \frac{C_\rho}{x^2} + \frac{C_\rho'}{x^{K_C}} \cos(\pi x + \phi), \quad (8)$$

which, from bosonization [13,27,28], is the expected behavior of a LE liquid with a spin gap and a charge Luttinger exponent K_c. (By contrast, a CDW insulator with a spin gap would definitionally exhibit long-range order at long distances, $C(x) \sim m^2 e^{i\pi x}$, where m is the order parameter, and should approach this asymptotic behavior exponentially.) As examples of the nature of the fits to Eq. (8) we have used to obtain K_C, in
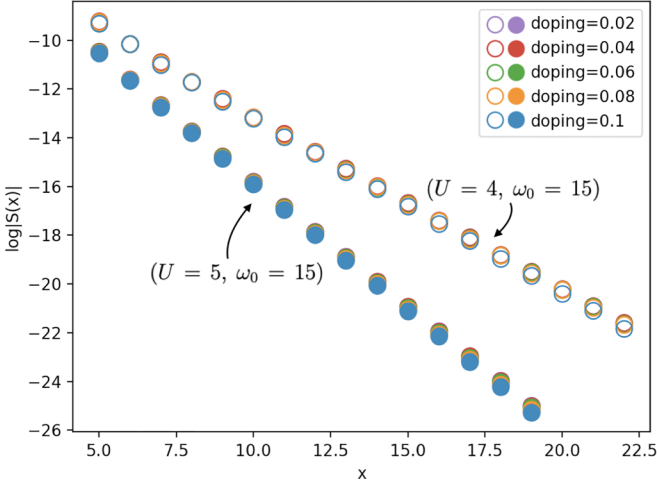
FIG. 7. Spin-spin correlation for $(U, \omega_0) = (4, 15)$ and $(5, 15)$ at different hole-doping concentrations from 0.02 to 0.1. We see for both values of (U, ω_0) that the spin correlations are essentially unchanged at different dopings.

Fig. 3 we show the results for $(U, \omega_0) = (6, 30)$ on a chain with $L = 200$. The dashed lines show the expected power-law behavior from Eq. (8), where, because we find a value of $K_c = 1.13 < 2$, we can ignore the nonoscillatory contribution (i.e., we set $C_\rho = 0$).

The values of K_C we have obtained as a function of ω_0 for all the values of U we have considered are shown in Fig. 4. In the limit $\omega_0 \to \infty$, since the Holstein model maps to the attractive Hubbard model, which has a charge SU(2) symmetry, the value of K_C must approach 1, as can be seen in Fig. 4. However, for a large but finite ω_0, we find $K_C > 1$ for all parameters we have considered.
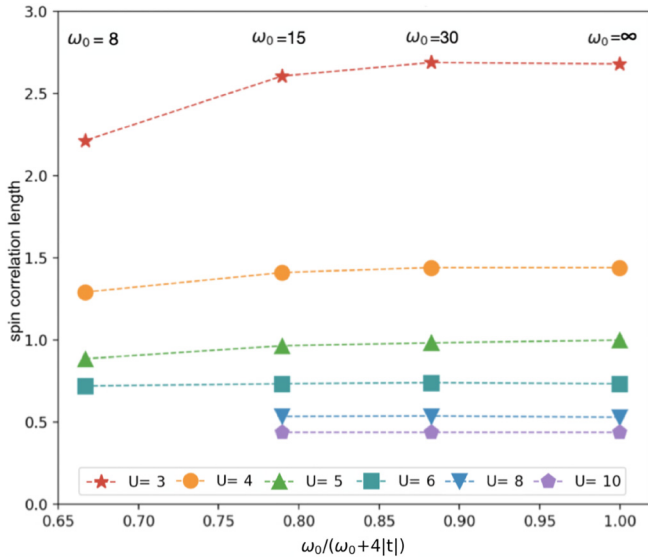

FIG. 8. A summary of the spin correlation lengths for all values of (U, ω_0).
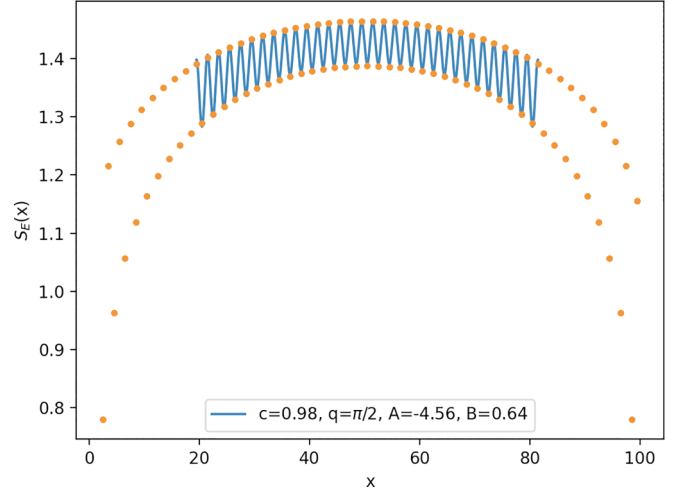

FIG. 9. Here we use $U = 3$ and $\omega_0 = 8$ as an example. We fit the middle part of the system with Eq. (8), as shown by the solid blue line. The extracted values of parameters are shown in the legend.

C. von Neumann entanglement entropy

To confirm that the system indeed has one gapless mode, we also calculate the von Neumann entanglement entropy $S_E(x) = -\text{tr}(\rho_x \ln \rho_x)$, where ρ_x is the reduced density matrix of a subsystem with length x. As was established in [29,30], for a (1+1)-dimensional system with open boundary conditions described by a conformal field theory,

$$S_E(x) = \frac{c}{6} \ln \left[\frac{4(L+1)}{\pi} \sin \left(\frac{\pi(2x+1)}{2(L+1)} \right) |\sin q| \right]$$
$$+ \frac{A \sin[q(2x+1)]}{\frac{4(L+1)}{\pi} \sin \left(\frac{\pi(2x+1)}{2(L+1)} \right) |\sin q|} + B, \quad (9)$$

where L is the length of the system and c, q, A, and B are adjustable parameters. As expected, we find that extrapolated to the limit $L \to \infty$, these fits produce a central charge c consistent with the predicted value, $c = 1$, and $q = k_F$. The quality of the fits to Eq. (9) can be seen for representative parameters in Fig. 9; the precise values of c obtained from such fits for various ω_0 and U are shown in Fig. 5, where we have assumed that $q = k_F$. Within the error bars, in all cases $c = 1$.

D. Finite hole doping

We perform one more consistency check on our numerics. If the state at half filling is a CDW with long-range order, then upon light hole doping, $\delta \ll 1$, we generate a gas of widely separated solitons. For small δ, where they are far from each other (i.e., when $\delta \xi_{sp} \ll 1$, where ξ_{sp} is the spin correlation length), the solitons should interact only through an effective hard-core interaction. Thus, they should behave like spinless fermions. Since the system is now incommensurate, this should result in power-law CDW correlations with a wave vector $Q = \pi(1 + \delta)$ and with a Luttinger exponent $K_c \to 2$ as $\delta \to 0$. The result is a discontinuity of K_c at $\delta = 0$. On the other hand, if the system is in a LE phase where the commensurability lock-in is irrelevant, then K_c should be a

continuous function of δ as $\delta \to 0$. As shown in Fig. 6, K_c shows no sign of a discontinuity at $\delta = 0$.

Moreover, the spin correlation length as shown in Fig. 7 is essentially unchanged for different doping levels, which is as expected since doping makes little difference in the nature of the state in a LE liquid phase.

IV. THE ADIABATIC LIMIT, $\omega_0 \to 0$

For $\omega_0 = 0$, the phonons are static, and the problem reduces to a version of the Peierls problem, which can be exactly treated with a mean-field analysis. In other words, the ground state of the system can be obtained by optimizing the energy while varying the phonon coordinates. For all nonzero U, this leads to a long-range-ordered, fully gapped phase with a gap Δ_0 of magnitude $\Delta_0 \approx 4|t| \exp[-2\pi|t|/U]$ for small U. Moreover, it is easy to see that the CDW is stable for small nonzero ω_0 as long as $\omega_0 \ll \Delta_0$.

V. THE WEAK-COUPLING LIMIT, $U \to 0$

A. The Takayama–Lin-Liu–Maki model

For small U, the low-energy properties of the Holstein model can be characterized by an effective field theory [the Takayama–Lin-Liu–Maki (TLM) model] [26]. Importantly, this effective field theory can be extended to the case of small but finite ω_0, where it is identical to the one that arises from the Su-Schrieffer-Heeger model. Thus, the phase diagram must be the same in this range of parameters for the two models. An estimate of the phase boundary in this region can be made as follows: (i) Because the model is asymptotically free, the UV cutoff can be taken to infinity in such a way that the low-energy properties are independent of it. Therefore, the soliton creation energy, which is the energy to produce a discommensuration in the CDW order, can be expressed as

$$E_S = \Delta_0 \, F(\omega_0/\Delta_0), \quad (10)$$

independent of the cutoff energy (bandwidth). (ii) While the full form of the scaling function F is not known, the first two terms for the small argument have been computed [8,31],

$$F(x) = \frac{2}{\pi} - Ax + O(x^2), \quad (11)$$

where $A \approx 0.6$. (iii) Quantum melting of the CDW order is expected to occur with increasing ω_0 at the critical point,

$$\omega_0 = x_c \Delta_0, \quad (12)$$

where $F(x_c) = 0$. In other words, this is the point at which a quantum-fluctuation-driven commensurate-to-incommensurate transition occurs.

Thus, Eq. (12) defines the phase boundary between the LE and CDW phases in the lower left corner of the phase diagram, where $U \to 0$ and $\omega_0 \to 0$. In other words, the phase boundary approaches this corner as

$$\omega_0 = 4x_c|t| \exp[-2\pi|t|/U]. \quad (13)$$

Moreover, we can estimate x_c from the first two terms in the small x expansion of F_s, which gives $x_c \approx 2/(0.6\pi) \approx 1$.

B. The functional RG method

In Ref. [24], the weak-coupling limit of this problem was analyzed using a perturbative RG method [32,33], which consists of successive integration of electron momentum degrees of freedom for all Matsubara frequencies divided into multiple patches. Consistent with our proposed phase diagram, it is found that as for weak enough U, the system flows toward a LE fixed point [24] characterized by a gap in the spin sector but not in the charge sector. To the best of our understanding, the perturbative RG is controlled only for asymptotically weak U. We thus mention, but do not further analyze, the fact that when the same analysis is carried out for a range of U, it is found that for fixed ω_0, when U exceeds a nonvanishing critical value, the umklapp scattering becomes relevant, suggesting a transition to a phase with CDW long-range order.

VI. THE STRONG-COUPLING $U \to \infty$ limit

When the bipolaron binding energy is much larger than the electron energy scale ($|U| \gg |t|$), performing a strong-coupling expansion for the Holstein model with the transformed Hamiltonian (2) up to fourth order yields an effective (pseudospin) Hamiltonian [25]:

$$H_{\text{eff}} = \sum_i \left[t_1(J_i^+ J_{i+1}^- + J_i^- J_{i+1}^+) + t_2(J_i^+ J_{i+2}^- + J_i^- J_{i+2}^+) \right.$$
$$\left. + 2V_1\left(J_i^z J_{i+1}^z - \frac{1}{4}\right) + 2V_2\left(J_i^z J_{i+2}^z - \frac{1}{4}\right)\right], \quad (14)$$

where

$$J_j^+ = (-1)^j c_{j\uparrow}^+ c_{j\downarrow}^+, \quad J_j^- = (J_j^+)^\dagger, \quad J_j^z = \frac{1}{2}(n_{j\uparrow} + n_{j\downarrow} - 1). \quad (15)$$

These pseudospin operators satisfy an SU(2) algebra and form a spin-$\frac{1}{2}$ representation, where a doubly occupied site corresponds to an up pseudospin and an empty site corresponds to a down pseudospin [25].

In this expansion, the combination t and U comes out as the overall energy scale, and the only tuning parameter is the dimensionless retardation factor $S \equiv U/\omega_0$. In Fig. 10 we show the coefficients t_1, t_2, V_1, and V_2 as a function of S for a given value of U and t. Explicit expressions and a detailed evaluation of all coefficients are given in the Appendix C. In the anti-adiabatic limit ($S \to 0$), these values agree with those in the strong-coupling expansion of the attractive Hubbard model:

$$t_1 \xrightarrow{S \to 0} \frac{1}{4}\left(\frac{4t^2}{|U|} - \frac{16t^4}{|U|^3}\right),$$
$$t_2 \xrightarrow{S \to 0} \frac{1}{4}\frac{4t^4}{|U|^3},$$
$$V_1 \xrightarrow{S \to 0} t_1,$$
$$V_2 \xrightarrow{S \to 0} t_2. \quad (16)$$

In the opposite limit $S \to \infty$, only V_1 remains nonzero, and we obtain a classical lattice gas, which has a CDW ground state, as expected. With the coefficients determined, we then solve the effective pseudospin Hamiltonian (14) with DMRG
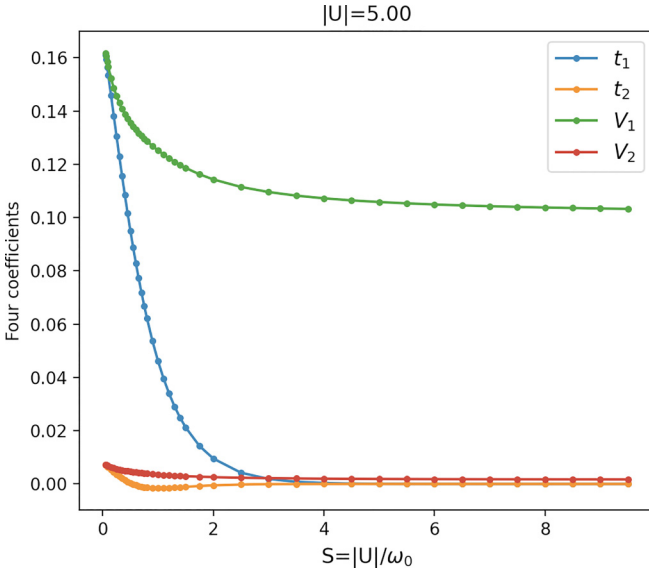
FIG. 10. An illustration of t_1, t_2, V_1, and V_2 as a function of the polaron band narrowing parameter $S = |U|/\omega_0$, with $t = 1$. Here we use $|U| = 5$ as an example.

and measure the spin-spin correlation function and the structure factor at $k = \pi$:

$$J(x) = \frac{1}{N_r} \sum_r \langle J^z(r) J^z(r+x) \rangle,$$

$$J(k = \pi) = \sum_x e^{i\pi x} J(x) = \sum_x (-1)^x J(x). \qquad (17)$$

Because the phase transition between the CDW and LE phases is a commensurate to incommensurate transition, when it is continuous, it should be in the Kosterlitz-Thouless (KT) university class. Therefore, in the CDW phase, we should see an antiferromagnetic pattern of pseudospin order and $J(k = \pi) \sim M^2 L$, with M being the order parameter approaching $\frac{1}{2}$ as ω_0 decreases. And in the LE liquid phase, the spin-spin correlation should exhibit power-law behavior $J(k = \pi) \sim L^{1-\eta}$, where $\eta > 1/4$, such that $\eta \to 1/4$ upon approaching the transition point. In this spirit, we plot $L(k = \pi)/L^{3/4}$ for $L = 100, 150, 300$. As shown in Fig. 11, there is a clear crossing point at $\omega_0 \approx 67$ for $L(k = \pi)/L^{3/4}$ with different L, which thus confirms the existence of a KT transition between the CDW and LE phases in the strong-coupling limit.

VII. OTHER NUMERICAL RESULTS

In the lower left corner of Fig. 1, A–G refer to a few calculations (not our own) by various numerical methods. The model at points A ($U = 0.6$, $\omega_0 = 0.5$), C (1.2, 0.5), D (1.62, 1.2), and E (1.62, 0.4) were studied using QMC continuous-time interaction expansion (CT-INT) method, with A and C at a temperature such that $\beta t = 50$, while for D and E $\beta t = 20$ [13]. On the basis of these studies, it was inferred that A is in the LE phase, while C, D, and E are in the CDW phase. On the basis of an early DMRG study, it was concluded that point F (2, 1) is in a CDW phase [12]. The two remaining points, B (1.0, 0.5) and G (3, 5), were identified as quantum critical points using a stochastic series expansion
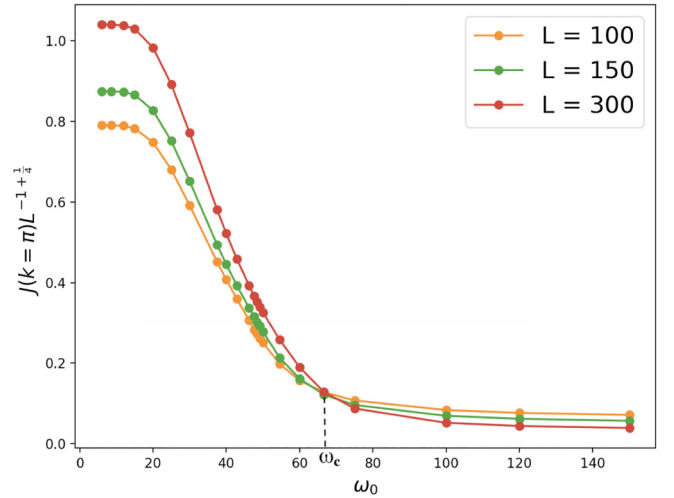

FIG. 11. Determining the position of the phase boundary at strong coupling. (We use data for $|U| = 30$ for illustrative purposes.) The finite-size scaling properties of the structure factor $J(k) = \sum_x e^{ikx} J(x)$ evaluated at $k = \pi$ are used to identify the critical value of ω_0, where $J(x)$ is the pseudospin correlation defined as in Eq. (17). In the ordered phase, $J(k) \sim M^2 L^2$, while in the disordered phase $J(k) \sim L^{1-\eta}$, where $\eta > 1/4$ such that $\eta \to 1/4$ upon approaching the KT transition. The clear crossing point in this plot establishes the existence of a KT transition between the CDW and LE phases with an estimated value of the critical $\omega_0 \approx 67$.

quantum Monte Carlo method [15], augmented by a finite-size scaling analysis.

There are manifestly some discrepancies between the conclusions drawn on the basis of these different numerical studies. Similarly, the smooth dotted line for the phase boundary shown in Fig. 1 is somewhat to the right of the optimal phase boundary one might draw on the basis of the earlier numerics. Due to the rather high temperature at which the QMC studies were conducted in comparison to the theoretically expected exponentially small CDW gap, we think that while these results may be qualitatively right, it should be expected that they will not be quantitatively precise. In any case, it is presently unclear whether the detailed shape of this phase boundary should be adjusted to better accommodate the results of contemporary numerical studies or one should stick to the present smooth interpolation and attribute the discrepancies to numerical uncertainty.

VIII. DISCUSSION OF THE PHASES OF THE DOPED SYSTEM

Slightly away from half filling, it is likely that there is a single LE phase everywhere in the phase diagram. The spin gap that characterizes both phases of the half-filled system is expected to extend smoothly to the lightly doped system. On the other hand, the generalized Luttinger theorem ensures that for an incommensurate electron density, there must be a gapless mode at $2k_F$. Thus, the only plausible phase is a LE liquid with a spin-gap and power-law CDW correlations.

There is one subtlety here worth noting. For $\omega_0 = 0$, slight doping is expected to produce a state consisting of an array

of solitons or discommensurations [8]. These will produce mid-gap states, resulting in a spin gap that is half the value of the spin gap in the undoped system. Upon including quantum fluctuations (i.e., for small but nonzero ω_0) the soliton lattice will melt to form a power-law phase with $K_c = 2$ (corresponding to dilute hard-core bosons or spinless fermions), but the spin gap is expected to be largely unaffected.

It is also possible that at larger deviations from half filling, CDW order with higher-order commensurability, for example, for the 1/3 filled band, can arise, especially in the small-ω_0 limit.

IX. CONCLUSIONS

Our major finding is the phase diagram in Fig. 1. The topology of the phase diagram rests on general arguments, although the possibility of additional phases at intermediate U/t and ω_0/t has not been definitively excluded. Moreover, the asymptotic forms of the phase boundary in the upper and lower corners of the phase diagram have been supported by what we believe to be a convincing analysis. The dotted part of the phase diagram is a sketch, drawn to smoothly connect with the established results in the asymptotic regimes. The quantitative disagreements between this sketch and some of the earlier numerical results (indicated by the gray points in Fig. 1) either may reflect some quantitative uncertainty in those results or may imply a more convoluted shape to the phase boundary.

The phase transition between the CDW and LE phases is a commensurate to incommensurate transition, so where it is continuous it should be described by a (1+1)-dimensional sine-Gordon theory and should thus be in the Kosterlitz-Thouless universality class. This has been verified by the strong-coupling calculations in the upper right corner of the phase diagram. However, it is not precluded that it could be first order along other parts of its extent.

ACKNOWLEDGMENTS

APPENDIX A: EFFECTIVE HAMILTONIAN IN THE ANTIADIABATIC LIMIT

In this Appendix, we provide details on the derivation of the effective Hamiltonian that provides the first corrections around the antiadiabatic limit, $\omega_0 \to \infty$. We do this in two ways, first via a path integral technique and then with Hamiltonian methods.

1. Path integral approach

In path integral language, the Euclidean action is

$$S[\psi^\dagger, \psi, v]$$

$$= \int_0^\beta d\tau \left\{ \sum_{ij} \psi_{i\sigma}^\dagger [(\partial_\tau + \mu)\delta_{ij} + t_{ij}]\psi_{j\sigma} \right.$$

$$\left. + \sum_i \left[\frac{M}{2}(\partial_\tau v_i)^2 + \frac{K}{2}v_i^2 \right] + \alpha \sum_i v_i \psi_{i\sigma}^\dagger \psi_{i\sigma} \right\} \quad (A1)$$

$$= \sum_n \left\{ \sum_{ij} \psi_{i\sigma,n}^\dagger [(i\omega_n + \mu)\delta_{ij} + t_{ij}]\psi_{j\sigma,n} \right.$$

$$\left. + \frac{1}{2}\sum_i v_{i,-n}(Mv_n^2 + K)v_{i,n} + \alpha \sum_i v_{i,-n}\rho_{i\sigma,n} \right\}. \quad (A2)$$

In the second line we transform to Matsubara frequencies $\omega_n = (2n+1)\pi/\beta$ and $v_n = 2n\pi/\beta$, and we define the density $\rho_{i\sigma} = \psi_{i\sigma}^\dagger \psi_{i\sigma}$. The phonon Green's function is

$$D(v_n) = \frac{1}{Mv_n^2 + K} = \frac{1}{K}\frac{\omega_0^2}{v_n^2 + \omega_0^2} \to \begin{cases} \delta_{v_n,0}/K & \omega_0 \to 0, \\ 1/K & \omega_0 \to \infty. \end{cases} \quad (A3)$$

Integrating out the phonon fields yields a retarded electron-electron interaction:

$$S_{\text{int}}[\psi^\dagger, \psi] = -\frac{\alpha^2}{2}\sum_n \sum_{i\sigma} \rho_{i\sigma,-n}D(v_n)\rho_{i\sigma,n}$$

$$= -\frac{\alpha^2}{2K}\sum_n \sum_{i\sigma} \rho_{i\sigma,-n}\left(\frac{\omega_0^2}{v_n^2 + \omega_0^2}\right)\rho_{i\sigma,n}. \quad (A4)$$

For $\omega_0 = \infty$, the interaction is instantaneous, and we recover the attractive Hubbard model with $U = \alpha^2/K$. We can expand around this limit in powers of $1/\omega_0$. This is equivalent to a gradient expansion in imaginary-time derivatives. The result is

$$S_{\text{int}} = -\frac{U}{2}\sum_n \sum_{i\sigma} \rho_{i\sigma,-n}\rho_{i\sigma,n} + \frac{U}{2\omega_0^2}\sum_n \sum_{i\sigma} \rho_{i\sigma,-n}v_n^2\rho_{i\sigma,n}$$

$$+ O\left(\frac{1}{\omega_0^4}\right). \quad (A5)$$

In imaginary time, the second term is

$$S_{\text{int}}^{(2)} = -\frac{U}{2\omega_0^2}\int_0^\beta d\tau \sum_{i\sigma}(\partial_\tau \rho_{i\sigma})^2. \quad (A6)$$

2. Hamiltonian approach

For a Hamiltonian approach, consider a unitary transformation of the Hamiltonian

$$H' = UHU^\dagger, \quad U = \prod_i e^{i\alpha p_i n_i/K}, \quad (A7)$$

where $\rho_i = \sum_\sigma \rho_{i\sigma} = \sum_\sigma c_{i\sigma}^\dagger c_{i\sigma}$. The result is

$$H' = -\sum_{ij} t_{ij}e^{i\alpha(p_i - p_j)/K}c_{i\sigma}^\dagger c_{j\sigma} - \frac{U}{2}\sum_i \rho_i^2 + \sum_i \frac{p_i^2}{2M}u + \frac{K}{2}v_i^2. \quad (A8)$$

The transformation removes the bilinear electron-phonon coupling at the cost of introducing an attractive electron-electron interaction and adding electron-phonon interaction into the hopping matrix elements. To find an expansion around $\omega_0 = \infty$, we rewrite the phonon coordinates and conjugate momenta in terms of the creation and annihilation operators,

$$p = i\sqrt{M\omega_0/2}(b^\dagger - b) \Rightarrow e^{i\alpha p/K} = e^{-\sqrt{U/(2\omega_0)}(b^\dagger - b)}, \quad \text{(A9)}$$

so that we may expand

$$H' \approx -\sum_{ij} t_{ij}\left\{1 + \sqrt{\frac{U}{2\omega_0}}[(b_j - b_j^\dagger) - (b_i - b_i^\dagger)]\right\}c_{i\sigma}^\dagger c_{j\sigma}$$
$$- \frac{U}{2}\sum_i \rho_i^2 + \omega_0\sum_i(b_i^\dagger b_i + 1/2). \quad \text{(A10)}$$

Specializing to the case of nearest-neighbor hopping, this expansion yields a coupling between the conjugate momentum of the phonon and the "lattice divergence" of the current:

$$\tilde{H}_{\text{int}}^{(2)} = \sqrt{\frac{U}{2\omega_0}}\sum_{n\sigma} i(b_n - b_n^\dagger)(j_n - j_{n-1}), \quad \text{(A11)}$$

where the local current operator is

$$j_n = it(c_n^\dagger c_{n+1} - c_{n+1}^\dagger c_n). \quad \text{(A12)}$$

In momentum space,

$$\tilde{H}_{\text{int}}^{(2)} = \sqrt{\frac{U}{2N\omega_0}}t\sum_{kq\sigma} f_{kq}(b_q - b_{-q}^\dagger)c_{k+q\sigma}^\dagger c_{k\sigma}, \quad \text{(A13)}$$

where

$$f_{kq} = -2i[\cos(k+q) - \cos k]. \quad \text{(A14)}$$

Direct perturbation theory about the $\omega_0 = \infty$ limits yields the effective electron-electron interaction:

$$H_{\text{int}}^{(2)} = -\frac{U}{N}\left(\frac{t}{\omega_0}\right)^2 \sum_{kq} V_{kk'q}c_{k+q\sigma}^\dagger c_{k\sigma}c_{k'-q\sigma'}^\dagger c_{k'\sigma'}, \quad \text{(A15)}$$

where

$$V_{kk'q} = f_{k,q}f_{k',-q} = -4(1 - \cos q)[\cos(k+k')$$
$$- \cos(k - k' + q)]. \quad \text{(A16)}$$

The continuity equation relates Eqs. (A15) and (A6).

APPENDIX B: THE ADIABATIC LIMIT $\omega_0 \to 0$ (DERIVATION FOR THE TLM MODEL)

Takayama, Lin-Liu, and Maki (TLM) found a remarkable analytic solution for solitons in a condensed CDW system, and their model is a continuum version of the Su-Schrieffer-Heeger model [8,35,36]. With similar treatment, we find in the continuum limit the effective field theory of the Holstein model is also the TLM model. The following is a short derivation. The Holstein model is defined as

$$H = -t\sum_{n,\sigma}(c_{n\sigma}^\dagger C_{n+1,\sigma} + \text{H.c.}) - \lambda\sum_{n,\sigma}x_n n_{n\sigma}$$
$$+ \frac{1}{2}K\sum_n x_n^2 + \frac{1}{2}M\sum_n \dot{x}_n^2. \quad \text{(B1)}$$

Let

$$x_n = e^{i\pi n}z_n. \quad \text{(B2)}$$

Then the coupling term becomes

$$\lambda\sum_{n,\sigma}(-1)^n z_n c_{n,\sigma}^\dagger c_{n,\sigma} = \lambda\sum_{n,\sigma}\sum_{kqq'} z_k\, e^{ikn}e^{i\pi n}e^{iqn}e^{-iq'n}c_{q,\sigma}^\dagger c_{q',\sigma}$$
$$= \lambda\sum_{kqq',\sigma} z_k\, c_{q,\sigma}^\dagger c_{q',\sigma}\delta_{k+\pi+q-q'}$$
$$= \lambda\sum_{kq,\sigma} z_k\, c_{q,\sigma}^\dagger c_{\pi+k+q,\sigma}. \quad \text{(B3)}$$

Now let $p = q - \frac{\pi}{2}$ and $p' = q' + \frac{\pi}{2}$,

$$\lambda\sum_{kq,\sigma} z_k\, c_{q,\sigma}^\dagger c_{\pi+k+q,\sigma}$$
$$= \lambda\sum_{k,|p|<\frac{\pi}{2},\sigma} z_k\, c_{k_F+p,\sigma}^\dagger c_{-k_F+k+p,\sigma}$$
$$+ \lambda\sum_{k,|p|<\frac{\pi}{2},\sigma} z_k\, c_{-k_F+p,\sigma}^\dagger c_{k_F+k+p,\sigma}$$
$$= \int dx\, \lambda z(x)[L_\sigma^\dagger(x)R_\sigma(x) + R_\sigma^\dagger(x)L_\sigma(x)]. \quad \text{(B4)}$$

The free-fermion part is (we set $\hbar = v_F = 1$)

$$H_0 = \sum_\sigma \int dx\, -(R_\sigma^\dagger i\partial_x R_\sigma - L_\sigma^\dagger i\partial_x L_\sigma)$$
$$= \sum_\sigma \int dx\, \psi_\sigma^\dagger(x)[-i\sigma_z\partial_x]\psi_\sigma(x), \quad \text{(B5)}$$

where $\psi_\sigma(x)$ is a spinor made up of the right-moving $R_\sigma(x)$ and left-moving $L_\sigma(x)$ components of the Fermi field near the

FIG. 12. The second-order and fourth-order diagrams used in the determination of the effective Hamiltonian. Reproduced from Ref. [25].

Fermi points. And the free-phonon part is

$$\frac{1}{2}K\sum_n x_n^2 + \frac{1}{2}M\sum_n \dot{x}_n^2 = \frac{1}{2}K\sum_n e^{i2\pi n}z_n^2 + \frac{1}{2}M\sum_n e^{i2\pi n}\dot{z}_n^2. \tag{B6}$$

So in the continuum limit, the Holstein model is also the TLM model:

$$H = \int dx\, \psi^\dagger(x)[-i\sigma_z\partial_x]\psi(x) \; + \; \lambda z(x)\psi^\dagger(x)\sigma_x\psi(x)$$

$$+ \int dx\, K\left[\frac{\dot{z}(x)^2}{\omega_0^2} + z^2(x)\right]. \tag{B7}$$

APPENDIX C: THE STRONG-COUPLING $U \to \infty$ limit

The strong-coupling expansion for the 1D Holstein model can be schematically expressed as the diagrams in Fig. 12. Figure 12(a) denotes the hopping of an electron from site i to site j and then back to site i, which is the only possibility for the second-order term. Similarly, Figs. 12(b) and 12(c) represent two possible fourth-order processes, while the unlinked diagram is not included here since its contributions vanish.

Then with pseudospin operators defined as in Eq. (15), the corresponding terms in the effective Hamiltonian are [25]

$$H^{(2)} = \frac{1}{2}\sum_i \left[j_\perp^{(2)}(i)\frac{1}{2}(J_i^+ J_{i+1}^- + J_i^- J_{i+1}^+) + j_\parallel^{(2)}(i)\left(J_i^z J_{i+1}^z - \frac{1}{4}\right)\right], \tag{C1}$$

$$H^{(4)} = \frac{1}{2}\sum_i \left[(j_\perp^{(4)}(i) + j_\perp'(i))\frac{1}{2}(J_i^+ J_{i+1}^- + J_i^- J_{i+1}^+) + j_\perp''(i)\frac{1}{2}(J_i^+ J_{i+2}^- + J_i^- J_{i+2}^+) \right.$$

$$\left. + (j_\parallel^{(4)}(i) - j_\parallel'(i))\left(J_i^z J_{i+1}^z - \frac{1}{4}\right) + (j_\parallel'(i) + j_\parallel''(i))\left(J_i^z J_{i+2}^z - \frac{1}{4}\right)\right], \tag{C2}$$

where the explicit expressions for eight coefficients are [25]

$$j_\perp^{(2)} = -2\left(-\frac{2t^2}{|U|}e^{-2S}\right)\left(1 + \sum_{n=1}^\infty \frac{S^n}{(S+1)(S+2)\cdots(S+n)}\right), \tag{C3}$$

$$j_\parallel^{(2)} = -2\left(-\frac{2t^2}{|U|}\right)\left(1 + \sum_{n=1}^\infty \frac{(-S)^n}{(S+1)(S+2)\cdots(S+n)}\right),$$

$$j_\perp^{(4)} = \frac{8t^4}{|U|^3}S^3 e^{-2S}\left[\sum_{\substack{m,m'=0 \\ m+m'\neq 0}}^\infty \int_0^1 dx \int_0^1 dy\, (xy)^{S-1}\, 2\cosh[S(x-y)]\frac{(S/2)^{m+m'}(1-x^2)^m(1-y^2)^{m'}}{m!m'!(m+m')}\right.$$

$$\left. - \sum_{m,m'=0}^\infty \frac{S^{m+m'}}{m!m'!}\frac{(-1)^m + (-1)^{m'}}{(m+S)^2(m'+S)}\right], \tag{C4}$$

$$j_\parallel^{(4)} = \frac{8t^4}{|U|^3}S^3 e^{-2S}\left[\sum_{\substack{m,m'=0 \\ m+m'\neq 0}}^\infty \int_0^1 dx \int_0^1 dy\, (xy)^{S-1}\left(e^{S(x+y)}\frac{(S/2)^{m+m'}(1-x)^{2m}(1-y)^{2m'}}{m!m'!(m+m')}\right.\right.$$

$$\left.\left. + e^{-S(x+y)}\frac{(S/2)^{m+m'}(1+x)^{2m}(1+y)^{2m'}}{m!m'!(m+m')}\right) - \sum_{m,m'=0}^\infty \frac{S^{m+m'}}{m!m'!}\frac{1+(-1)^{m+m'}}{(m+S)^2(m'+S)}\right], \tag{C5}$$

$$j_\perp' = \frac{4t^4}{|U|^3}S^3 e^{-2S}\left[\int_0^1 dx \int_0^1 dy \int_0^1 dz(xyz)^{S-1}\left(\exp\left\{\frac{S}{2}[x-y+z-2z(x-y)-xyz]\right\} + \exp\left\{\frac{S}{2}[x-y-z(x+y)]\right\}\right)\right.$$

$$\left. + 2\int_0^1 dx \int_0^1 dy(xy)^{S-1}e^{S(x-y)}\sum_{m=1}^\infty \frac{(S/2)^m(1-x)^m(1+y)^m}{m!m} + \int_0^1 dx \int_0^1 dy(xy)^{S-1}e^{S(x-y)}(\ln x + \ln y)\right], \tag{C6}$$

$$j_\perp'' = -\frac{4t^4}{|U|^3}S^3 e^{-2S}\left[\int_0^1 dx \int_0^1 dy \int_0^1 dz(xyz)^{S-1}\exp\left\{\frac{1}{2}S[x+y+z-2z(x+y)+xyz]\right\}\right.$$

$$\left. + 2\int_0^1 dx \int_0^1 dy(xy)^{S-1}e^{-S(x+y)}\sum_{m=1}^\infty \frac{(S/2)^m(1+x)^m(1+y)^m}{m!m} + 2\int_0^1 dx \int_0^1 dy(xy)^{S-1}e^{-S(x+y)}\ln x\right], \tag{C7}$$

$$j_\parallel' = -\frac{4t^4}{|U|^3}S^3 e^{-2S}\left[\int_0^1 dx \int_0^1 dy \int_0^1 dz(xyz)^{S-1}\left(\exp\left\{\frac{S}{2}[-x-y+z+2z(x+y)+xyz]\right\}\right.\right.$$
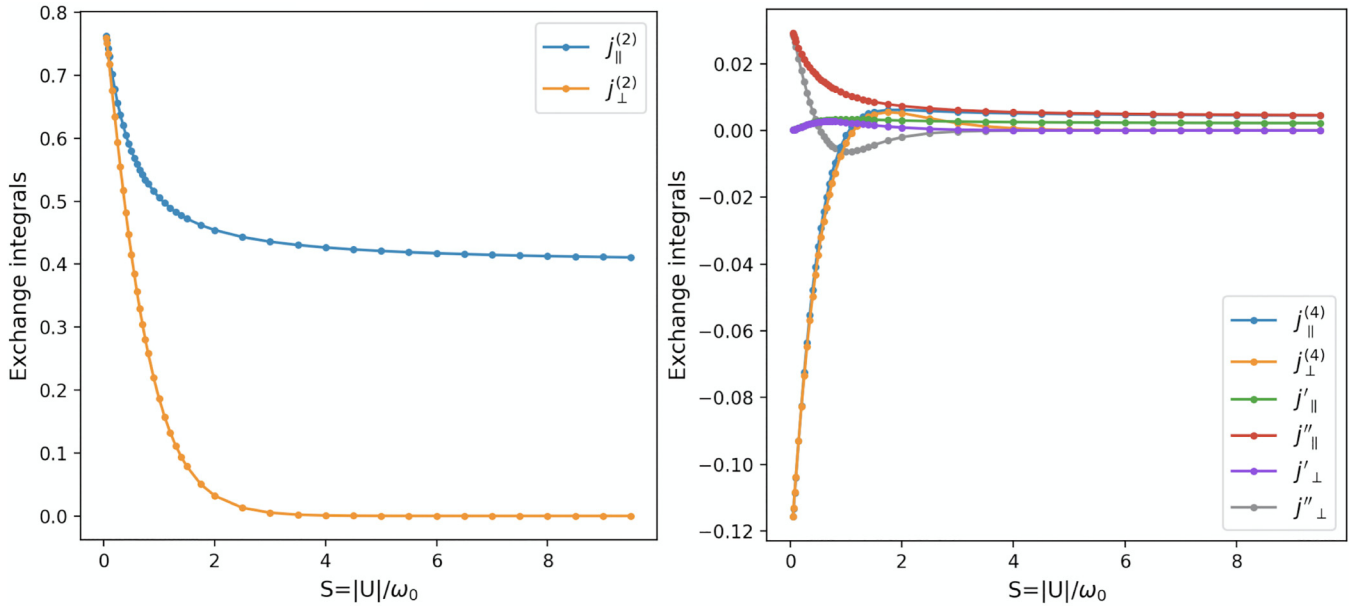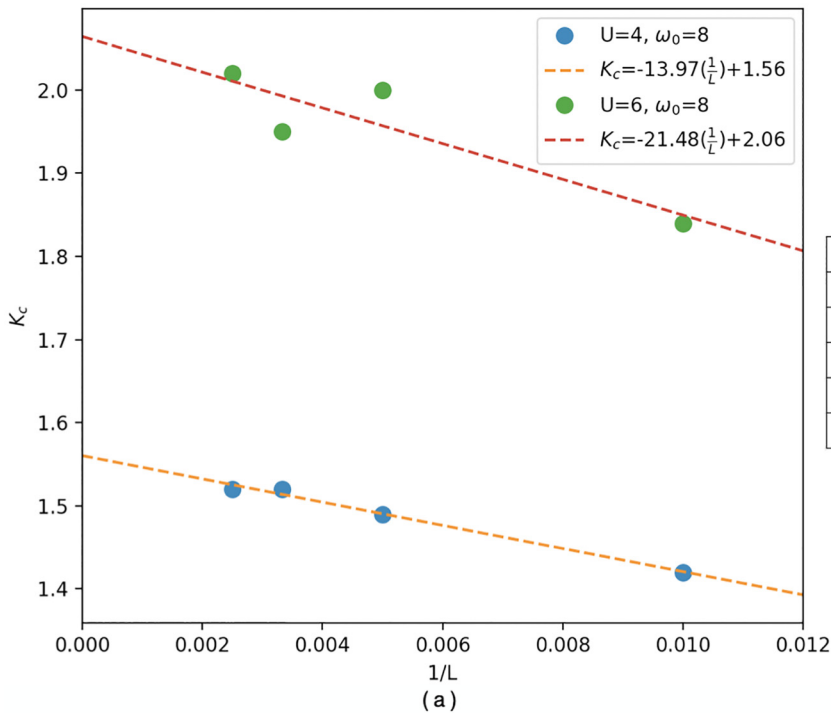
FIG. 13. An illustration of the exchange integrals (coefficients of the effective pseudospin Hamiltonian) as a function of S with $t = 1$. Here we use $|U| = 5$ as an example.

$$+ \exp\left\{\frac{S}{2}[-x - y + 2z + z(x + y) + 2xyz]\right\}\right)$$

$$+ 2\int_0^1 dx \int_0^1 dy \, (xy)^{S-1} e^{S(x+y)} \sum_{m=1}^{\infty} \frac{(S/2)^m (1-x)^m (1-y)^m}{m!m} + 2\int_0^1 dx \int_0^1 dy \, (xy)^{S-1} e^{S(x+y)} \ln x \right], \quad (C8)$$

$$j''_{\parallel} = \frac{4t^4}{|U|^3} S^3 e^{-2S} \int_0^1 dx \int_0^1 dy \int_0^1 dz \, (xyz)^{S-1} \exp\left\{\frac{1}{2}S[x + y + 2z - z(x + y) + 2xyz]\right\}. \quad (C9)$$

(U, ω_0)	E_{GS} for the middle 10 sites
U=3, ω_0=15	-2.160
U=4, ω_0=15	-2.540
U=5, ω_0=15	-2.951
U=6, ω_0=15	-3.384
U=8, ω_0=15	-4.291

(a)   (b)

FIG. 14. (a) Finite-size scaling analysis of K_C for $L \in [100, 200, 300, 400]$. Here we use $(U, \omega_0) = (4, 8)$ and $(6, 8)$ as examples. (b) Estimates of the ground-state energies per site for the middle 10 sites in various regimes.

Here the combination t and U comes out as the overall energy scale, and the only tuning parameter is the dimensionless retardation factor $S \equiv U/\omega_0$. We evaluate the values of eight coefficients as a function of S, as shown in Fig. 13. Then t_1, t_2, V_1, and V_2 can be determined through Eq. (C10) and are plotted in Fig. 10. We see at finite $|U|$ that, as $S \to 0$, i.e., $\omega_0 \to \infty$ (the Hubbard limit), the values of t_1, t_2, V_1, and V_2 match the analytic expressions given in Eq. (16):

$$t_1 = \frac{1}{4}\big[j_\perp^{(2)}(i) + j_\perp^{(4)}(i) + j_\perp'(i)\big] \xrightarrow{\omega_0 \to \infty} \frac{1}{4}\left(\frac{4t^2}{|U|} - \frac{16t^4}{|U|^3}\right), \quad t_2 = \frac{1}{4}j_\perp''(i) \xrightarrow{\omega_0 \to \infty} \frac{1}{4}\frac{4t^4}{|U|^3},$$

$$V_1 = \frac{1}{4}\big[j_\parallel^{(2)}(i) + j_\parallel^{(4)}(i) - j_\parallel'(i)\big] \xrightarrow{\omega_0 \to \infty} t_1, \quad V_2 = \frac{1}{4}\big[j_\parallel'(i) + j_\parallel''(i)\big] \xrightarrow{\omega_0 \to \infty} t_2. \tag{C10}$$

APPENDIX D: ADDITIONAL CALCULATIONS

In Fig. 14(a), we show an example of the finite-size scaling analysis we used to extract the Luttinger exponent K_c. The system sizes accessible to us are very long (up to 400 unit cells). Further, the Luttinger exponent is extracted from the correlation function data extrapolated to infinite system size L, assuming the leading correction is proportional to $1/L$. In Fig. 14(b), we provide a table with the ground-state energies per site for the middle 10 sites computed with DMRG.

[1] R. Peierls, *Surprises in Theoretical Physics* (Princeton University Press, Princeton, NJ, 1979).

[2] J.-P. Pouget, The Peierls instability and charge density wave in one-dimensional electronic conductors, C. R. Phys. **17**, 332 (2016).

[3] M. Hohenadler and H. Fehske, Density waves in strongly correlated quantum chains, Eur. Phys. J. B **91**, 204 (2018).

[4] L. D. Landau, The movement of electrons in the crystal lattice, Phys. Z. Sowjetunion **3**, 644 (1933).

[5] T. Holstein, Studies of polaron motion: Part I. The molecular-crystal model, Ann. Phys. (NY) **8**, 325 (1959).

[6] T. Holstein, Studies of polaron motion: Part II. The "small" polaron, Ann. Phys. (NY) **8**, 343 (1959).

[7] A. Alvermann, H. Fehske, and S. A. Trugman, Polarons and slow quantum phonons, Phys. Rev. B **81**, 165113 (2010).

[8] A. J. Heeger, S. Kivelson, J. R. Schrieffer, and W. P. Su, Solitons in conducting polymers, Rev. Mod. Phys. **60**, 781 (1988).

[9] H. Fehske, G. Hager, and E. Jeckelmann, Metallicity in the half-filled Holstein-Hubbard model, Europhys. Lett. **84**, 57001 (2008).

[10] S. Ejima and H. Fehske, DMRG analysis of the SDW-CDW crossover region in the 1D half-filled Hubbard-Holstein model, J. Phys.: Conf. Ser. **200**, 012031 (2010).

[11] M. Tezuka, R. Arita, and H. Aoki, Phase diagram for the one-dimensional Hubbard-Holstein model: A density-matrix renormalization group study, Phys. Rev. B **76**, 155114 (2007).

[12] E. Jeckelmann, C. Zhang, and S. R. White, Metal-insulator transition in the one-dimensional Holstein model at half filling, Phys. Rev. B **60**, 7950 (1999).

[13] J. Greitemann, S. Hesselmann, S. Wessel, F. F. Assaad, and M. Hohenadler, Finite-size effects in Luther-Emery phases of Holstein and Hubbard models, Phys. Rev. B **92**, 245132 (2015).

[14] M. Hohenadler and F. F. Assaad, Excitation spectra and spin gap of the half-filled Holstein-Hubbard model, Phys. Rev. B **87**, 075149 (2013).

[15] R. T. Clay and R. P. Hardikar, Intermediate Phase of the One Dimensional Half-Filled Hubbard-Holstein Model, Phys. Rev. Lett. **95**, 096401 (2005).

[16] R. P. Hardikar and R. T. Clay, Phase diagram of the one-dimensional Hubbard-Holstein model at half and quarter filling, Phys. Rev. B **75**, 245103 (2007).

[17] J. E. Hirsch and E. Fradkin, Phase diagram of one-dimensional electron-phonon systems. II. The molecular-crystal model, Phys. Rev. B **27**, 4302 (1983).

[18] K.-M. Tam, S.-W. Tsai, and D. K. Campbell, Validity of the Tomonaga Luttinger liquid relations for the one-dimensional holstein model, Phys. Rev. B **84**, 165123 (2011).

[19] H. Fehske, G. Wellein, A. Weiße, F. Göhmann, H. Büttner, and A. R. Bishop, Peierls-insulator Mott-insulator transition in 1D, Phys. B (Amsterdam, Neth.) **312–313**, 562 (2002).

[20] H. Fehske, A. P. Kampf, M. Sekania, and G. Wellein, Nature of the Peierls- to Mott-insulator transition in 1D, Eur. Phys. J. B **31**, 11 (2003).

[21] H. Fehske, G. Wellein, G. Hager, A. Weiße, and A. R. Bishop, Quantum lattice dynamical effects on single-particle excitations in one-dimensional Mott and Peierls insulators, Phys. Rev. B **69**, 165115 (2004).

[22] I. P. Bindloss, Phase diagram and isotope effects of the quasi-one-dimensional electron gas coupled to phonons, Phys. Rev. B **71**, 205113 (2005).

[23] H. Bakrim and C. Bourbonnais, Quantum vs classical aspects of one dimensional electron-phonon systems revisited by the renormalization group method, Phys. Rev. B **76**, 195115 (2007).

[24] H. Bakrim and C. Bourbonnais, Nature of ground states in one-dimensional electron-phonon Hubbard models at half filling, Phys. Rev. B **91**, 085114 (2015).

[25] J. K. Freericks, Strong-coupling expansions for the attractive Holstein and Hubbard models, Phys. Rev. B **48**, 3881 (1993).

[26] See Appendix B.

[27] T. Giamarchi, *Quantum Physics in One Dimension* (Oxford University Press, Oxford, 2004).

[28] J. Voit, One-dimensional Fermi liquids, Rep. Prog. Phys. **58**, 977 (1995).

[29] P. Calabrese and J. Cardy, Entanglement entropy and quantum field theory, J. Stat. Mech. (2004) P06002.

[30] M. Fagotti and P. Calabrese, Universal parity effects in the entanglement entropy of *XX* chains with open boundary conditions, J. Stat. Mech. (2011) P01017.

[31] M. Nakahara and K. Maki, Quantum corrections to solitons in polyacetylene, Phys. Rev. B **25**, 7789 (1982).

[32] G. T. Zimanyi, S. A. Kivelson, and A. Luther, Superconductivity from Predominantly Repulsive Interactions in Quasi One-Dimensional Systems, Phys. Rev. Lett. **60**, 2089 (1988).

[33] L. G. Caron and C. Bourbonnais, Two-cutoff renormalization and quantum versus classical aspects for the one-dimensional electron-phonon system, Phys. Rev. B **29**, 4230 (1984).

[34] M. Fishman, S. R. White, and E. M. Stoudenmire, The ITensor Software Library for tensor network calculations, SciPost Phys. Codebases **1**, 4 (2022).

[35] H. Takayama, Y. R. Lin-Liu, and K. Maki, Continuum model for solitons in polyacetylene, Phys. Rev. B **21**, 2388 (1980).

[36] B. Horovitz, Solitons in polyacetylene: A comment, Phys. Rev. B **22**, 1101 (1980).